Mapana – Journal of Sciences
2025, Vol. 24, No. 2, *87-101*
ISSN 0975-3303 | https://doi.org/10.12723/mjs.73.5

Design and Development of a Capacitance Sensor for Gas/Gas or Gas/Liquid Void Fraction Detection

V. Kesavan[*†], J. Jayachandiran[†] and D. Nedumaran[†]

Abstract

A capacitance-based void fraction sensor was designed to detect a range of liquids and gases. The sensor comprises two semi-concave copper electrodes mounted on a hollow cylindrical glass tube. When a radio frequency signal is applied, variations in the dielectric constant of the surrounding medium cause measurable phase shifts in the signal. Experiments with tap water, distilled water, and ethanol showed that the phase shift is directly correlated with the dielectric constant of the liquid. To study gas-phase behaviour, measurements were carried out under mesoporous conditions (10% liquid and 90% gas flow), allowing characterisation of gas molecules based on their dielectric responses. Signal variations were captured using a digital storage oscilloscope, and the observed phase shifts were compared with theoretical values computed using Mathematica. The experimental findings closely matched the theoretical predictions, validating the sensor's effectiveness in accurately detecting and monitoring liquid and gas flow in pipelines.

Keywords: Capacitance sensor, Two-phase flow, Void fraction, Phase-shift Gas/Liquid detection.

[*] West University of Timişoara, Bulevardul Vasile Pârvan 4, Timişoara-300223, Romania; kesavansilicon@gmail.com

[†] Central Instrumentation and Service Laboratory, University of Madras, Guindy Campus Chennai 600 025, TN, India; jayasid5@gmail.com; dnmaran@gmail.com

1. Introduction

Void fraction measurement in two-phase (gas-liquid) flow is crucial for various industries such as petrochemicals, chemical processing, soil mechanics and oil production. The void fraction significantly influences heat transfer, pressure drop and flow dynamics, making its precise determination essential for system design and operation. Currently, a range of measurement techniques are employed, such as gamma ray attenuation, capacitance sensors, electrical impedance methods and capacitance transducers, each offering different advantages depending on the application [1], [2], [3]. Void fraction is vital for understanding two-phase flows, determined by the dielectric constant, density and viscosity. These flows are typically assessed vertically or horizontally, with void fraction measured using geometric methods like local, cross-sectional, or volumetric approaches. Cross-sectional analysis compares phase areas, often using models based on flow physics or empirical methods to categorise void fractions.

M. Zubair and T. B. Tang have simulated and fabricated a capacitance sensor using the void fraction technique, reporting that the proposed system provides a portable solution for grading extremely pure crude oil [4]. The void proportion in two-phase flows was experimentally confirmed by another investigation utilising a DSO to measure the phase shift between the response signal from the capacitance sensor and a reference signal [5]. According to their results, the void fraction phase shift approach produces an additional uniform and steady signal than the capacitance measuring method. *Huang et al.* designed a stray capacitance sensor for industrial applications to measure stray-immune measurement [6]. *Schmidt J.W et al.* have accurately measured the dielectric permittivity of eight gases, such as He, Ar, N_2, O_2, CH_4, C_2H_6, C_3H_8 and CO_2, using cross capacitance and 16-rod capacitance for these studies [7].

Mesoporous materials are commonly employed in capacitive sensing applications, such as humidity sensors, due to their high surface area and tunable pore structure. In controlled laboratory environments, capacitive sensors are used to monitor changes in the dielectric permittivity of these materials, which vary in response to the concentration of a target gas. *Thorsten et al.* have designed a capacitive sensor based on a mesoporous silica pellet for measuring humidity from 90 °C to 210 °C, demonstrating its stability at high temperatures compared to organic polymers[8], [9]. Enhanced gas permeability was achieved by incorporating nano-sized mesoporous silica into mixed matrix membranes (MMMs) [8]. Specifically, various mesoporous fillers such as MCM-41 and MCM-48 were combined with a polysulfone (PSF) matrix at different concentrations. Notably, a

membrane consisting of PSF with 80% MCM-41 significantly increased the permeability of gases including helium (He), carbon dioxide (CO_2), oxygen (O_2), nitrogen (N_2) and methane (CH_4), with respective increases of 274.81%, 232.29%, 248.98%, 400.00% and 488%. Mesoporous silica was also utilised by *Thorsten Wagner et al.* in the design of capacitance-based humidity sensors, highlighting its low cost and high sensitivity to humidity [10].

A. Prim et al. have synthesised CaO-loaded In_2O_3 mesoporous materials, which were used as resistive gas sensors for the detection of CO_2 [11]. At the same time, Brian Y. and his colleagues designed a thin-film NO_2 gas sensor utilising mesoporous MCM-41 modified with tungsten and vanadium.[12]. The MCM-41-based gas sensor demonstrated high sensitivity for detecting NO_2 gas at low concentrations, down to several hundred parts per billion. *Yang, J. et al.* synthesised SiO_2@MCM-41 using a simple method and loaded it with $ZnCl_2$, SNP and hexamine as indicators. The SiO_2@MCM-41 demonstrated a rapid response, high sensitivity, excellent stability and perfect concentration-response linearity [13]. *Esmaeili, S. et al.* have designed a colorimetric sensor array using SiO_2@MCM-41 and SiO_2@Ti-MCM-41 for detecting various sensitive dyes and ammonia gas. This combination of the array has been effective for a wide range of concentrations [14]. *Ji Yang et al.* prepared MCM-41/PPy composites on a ceramic substrate for use in humidity sensors, demonstrating high sensitivity, good linearity and favourable stability [15].

In this work, we designed cross-capacitor-based sensors to measure gas/liquid and gas/gas void fractions. MCM-41 mesoporous pellets were used to increase the permeability of gases, aiding in accurately detecting gases in the gas/gas void fraction. Additionally, three capacitive sensors featuring concave copper electrodes of varying lengths were developed to measure the void fraction in two-phase flow systems. The measurement setup was constructed for gas-liquid and gas-gas systems. In the gas-liquid system, the void fraction between air, ethanol, distilled water and normal water was measured and calculated. For the gas-gas void fraction measurement system, mesoporous PSF with 80% MCM-41 was employed to measure the void fraction for He, CO_2, O_2, N_2 and CH_4. Changes in the void fraction between the two phases were measured through the phase shift method using DSO. The results indicated that the developed capacitance-based void fraction sensor could effectively detect liquid and gas flow through pipelines.

2. Experimental Set-up

2.1 Sensor Methodology

The void fraction of the two phases is calculated using the phase shift method. We primarily employed two operational amplifier (op-amp) phase shift circuits: one for the reference signal and another for measuring phase changes detected through alterations in dielectric values (permittivity). The capacitance of a two-electrode sensor is influenced by the effective dielectric permittivity within the pipeline between the concave electrodes, as well as by the material's resistivity[5]. Figure 1a illustrates the schematic diagram of the electrode mounted on a glass graduated cylinder for the capacitance sensor and Figure 1b shows the equivalent circuit of the sensor.

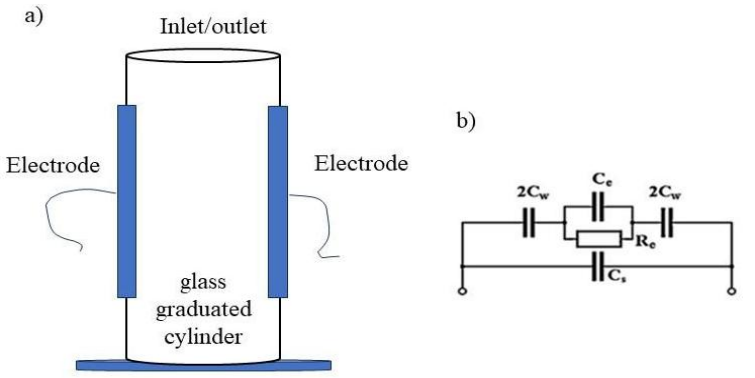

Figure 1. (a) The Schematic representation of the proposed capacitance sensor with a glass graduated cylinder and (b) its equivalent circuit.

The admittance between the two electrodes, the dielectric liquids, the void fraction variation calculation, the transmittance calculation in the ideal operational amplifier and the phase shift between the input reference signal and the output measuring signal have been calculated using the theory mentioned in *A. Jaworek et al.* [5].

The admittance between the two electrodes is represented as

$$Y = 1/(1/(1/R_e) + j\omega C_e) + (1/j\omega C_w) + j\omega C_s \quad (1)$$

The void fraction variations can be calculated using equations (2-4)

$$Y = \rho((C_w/C_{e0})/(1 + (C_w/C_e\varepsilon_{e0})) + (C_s/C_{e0})) \quad (2)$$

$$C_e = \varepsilon_0\varepsilon_e A/d \quad (3)$$

$$C_e = (\varepsilon_0 A/d)\varepsilon_e \quad (4)$$

Here $C_e = C_{e0}\varepsilon_e$ and for air filled within the glass graduated cylinder is represented by $\varepsilon_e = 1$, so $C_e = C_{e0}$. In addition, C_w denotes the wall capacitance, C_s represents the stray capacitance, and C_e stands for the effective capacitance corresponding to the medium inside the pipe. Similarly, R_e is the effective resistance of the medium within the glass graduated cylinder. In this work, Crystal quartz (SiO_2) has been used, and glass resistivity depends on the materials used and has an electrical resistivity of about $10^{18}\,\Omega m$ and a dielectric constant of 3.75 at $20\,°C\ at\ 1\,MHz$.

The Phase shift is calculated using Eq. (5),

$$\varphi = arctan\ arctan\ \frac{2(R_2/R_{e0})(lm(Y)/\omega C_{e0})\eta 0}{1-(R_2^2/R_{e0}^2)(((Y)R_{e0}^2+(\eta 0^2(\frac{lm^2(Y)}{\omega^2 C_{e0}^2})))} \quad (5)$$

2.2 Phase shift measurement setup for liquids

The measurement set-up comprises of 50 mL glass graduated cylinder with an inner diameter of 22 mm and an outer diameter of 25 mm. Two Copper concave electrodes were mounted on the pipeline with a 140° arc. The arc of the copper electrodes and the length of the electrodes were selected based on reference [5]. The inner diameter of the copper electrodes was fixed at 23 mm and various lengths were used for measurement: 20 mm, 40 mm, 70 mm and 110 mm. Figure 2a shows the schematic diagram of the electrode mounting, while the copper plates and the capacitance sensor circuit are shown in Figures 2b and 2c, respectively. The phase detection circuit comprises of IC-LF356 due to its advantageous features including low input bias, low response current and low offset voltage.

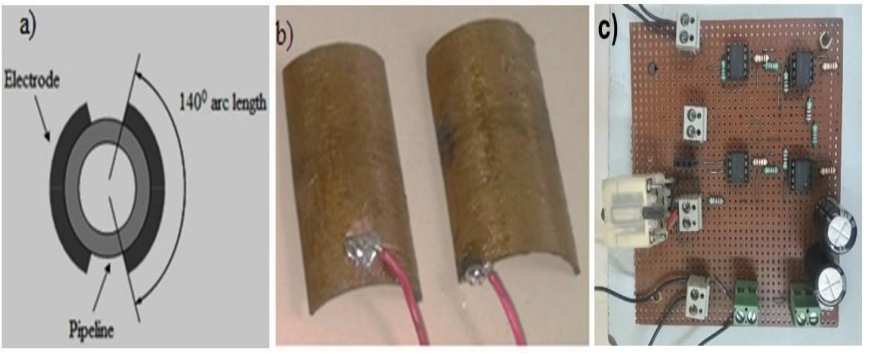

Figure 2. (a) The schematic diagram of the electrode mounting, (b) actual electrodes, and (c) capacitance sensor circuit.

In the initial stage, the glass cylinder is empty (filled with air), and the phase shift is assumed to be zero ($\Delta\varphi = 0$) due to the absence of a void fraction. The glass cylinder is then filled with different types of liquids, such as distilled water, normal water and ethanol. Measurements of the sensor response delay time were conducted for normal water, distilled water and ethanol using a DSO. The resistivity of distilled water is 2.5×10^4 Ωm, with a relative permittivity of 78.4 at 20 °C. The permittivity of ethanol and normal water is 24 and 81, respectively, while their resistivities are 2.29×10^3 Ωm and 5.0×10^3 Ωm. Mathematica software was used to calculate the real, imaginary and phase components of the admittance and delay time for the different liquids using Eq. (1-5). The permittivity of air is taken as 1 and the phase shift as 20°. The reference signal for the phase shift was set to 20°, resulting in a phase shift difference of zero between the reference signal and the phase detection signal. The phase shift was then calculated for distilled water, ethanol and normal water using capacitance plates of lengths 20 mm, 40 mm, 70 mm and 110 mm. The schematic diagram of the phase shift circuit is shown in Figure 3.

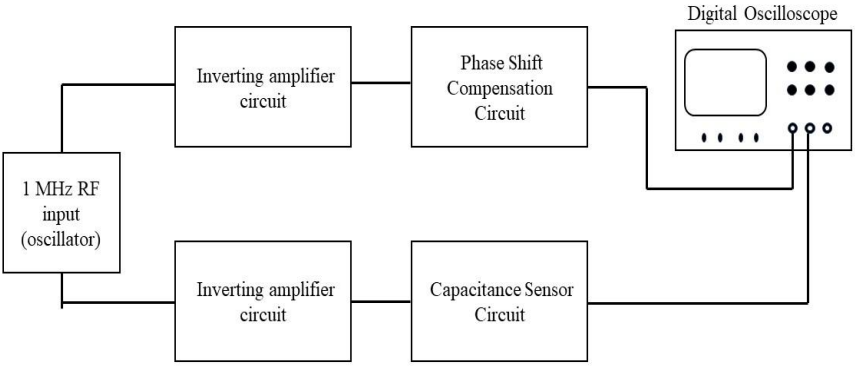

Figure 3. The Schematic diagram of the phase shift circuit.

Here, the Digital Oscilloscope Caddo 3025C was used for measuring the phase shift. A FALCON FG20DDS -20 MHz model function generator was used, with inputs set to 2 mV/div and 1 ns/div. The phase shift is calculated using equation (6).

$$\Delta\varphi = 2\pi \frac{\Delta t}{T}. \qquad (6)$$

were Δt is the time difference, and T is the total time. The total time to reach the peak amplitude is 1000 ns, and the time delay has been measured using the DSO.

2.3 Phase shift measurement set-up for gases

The phase shift was calculated for five gases: He, N_2, O_2, CH_4 and CO_2, but measurements were conducted only for three of these gases. Generally, gases have low permeability values, so membranes were used to increase permeability. *Sangil Kim et al.* fabricated mesoporous molecular sieves of polysulfone (PSF) with different percentages of mixed matrix membranes (MMMs-41) for gas separation purposes. They successfully increased the permeability of the five gases. The gas permeability of these five gases, before and after using 80% of MCM-41, is shown in Table 1. The membrane comprising 80% of MCM-41 with PSF increased the permeability of the gases by up to 488% [8]. The gas permeabilities of various gases before and after incorporating 80% MCM-41 are detailed in Table 1, as reported in the source [10]. *Prim, A et al.* has measured the CO_2 gas by using the Novel Mesoporous CaO- loaded In_2O_3 materials [11].

Table 1 Gas permeabilities of various gases: before and after using 80 % of MCM-41.

Membranes	**Vol % of MCM-41**	**He**	**CO_2**	**O_2**	**N_2**	**CH_4**
PSF	0	8.02	4.46	0.98	0.18	0.17
MCM-41/PSF	80	30.06 (274.81%)	14.82 (232.29%)	3.42 (248.98%)	0.90 (400.00%)	1.00 (488%)

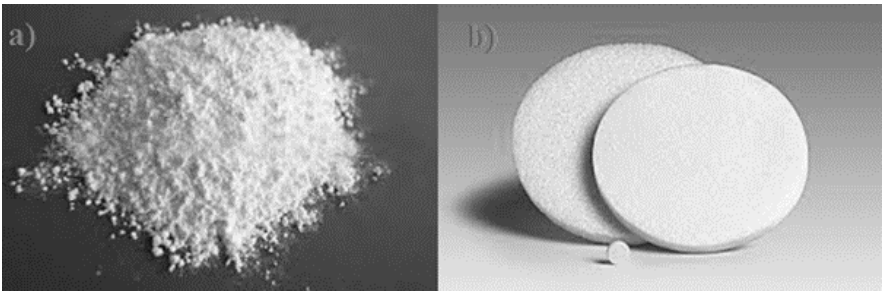

Figure 4. (a) MCM-41 powder and (b) pellets.

MCM-41 materials generally have low densities due to their porous structure, with densities ranging from 40-150 kg/m^3. Pelletizing is a widely used method for sample preparation, where solid materials are compacted into flat, circular pellets suitable for analytical techniques. In this case, a pellet was produced using MCM-41, measuring 0.016 mm in diameter and 0.005 mm in thickness. Laboratory equipment such as automatic hydraulic presses, including those operated by air pressure, is commonly employed to form these sample discs. The powder and pellet forms of MCM-41 are shown in Figures 4(a) and 4(b). A pellet is used to increase the dielectric constant because gases have low dielectric constant values, while also

providing a small phase shift between the reference signal and the capacitance sensing signal. The glass tube with porous pellets and the schematic diagram of the electrode mounted on the glass tube are shown in Figure 5.

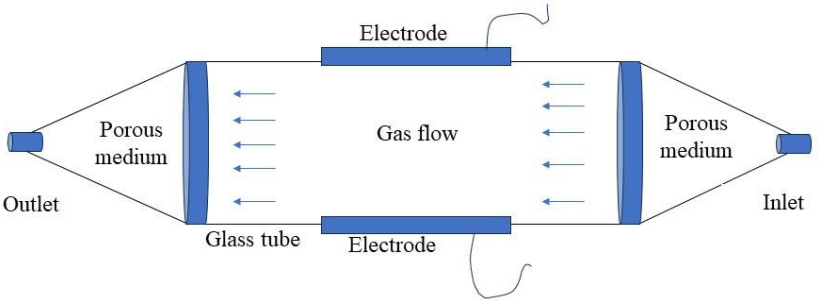

Figure 5. Schematic diagram of the electrode mounted on the glass tube with porous medium.

3. Results and Discussion

3.1 Phase-Shift Detection for Different Types of Liquids

The experimental setup of the capacitance sensor for measuring different types of liquids is shown in Figure 6. Figure 7 presents the phase shift output of air compared to distilled water using 40 mm electrodes, measured across various voltage and time scales for accurate phase shift assessment. Figure 7(a) illustrates the phase shift measurement between the air-filled (empty) capacitance signal and the reference signal, where the phase shift and void fraction are zero. This measurement was conducted using a 200 mV/div and 100 ns/div scale. Figure 7(b) shows the phase shift difference between air and normal water, using the same scale of 200 mV/div and 100 ns/div. Figure 7(c) displays the phase shift of normal water with a scale of 100 mV/div and 50 ns/div. Finally, Figure 7(d) illustrates the phase shift of normal water with a scale of 2 mV/div and 10 ns/div.

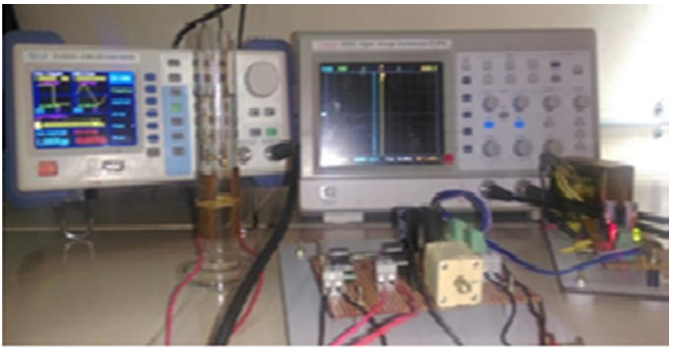

Figure 6. The Experimental setup of the capacitance sensor.

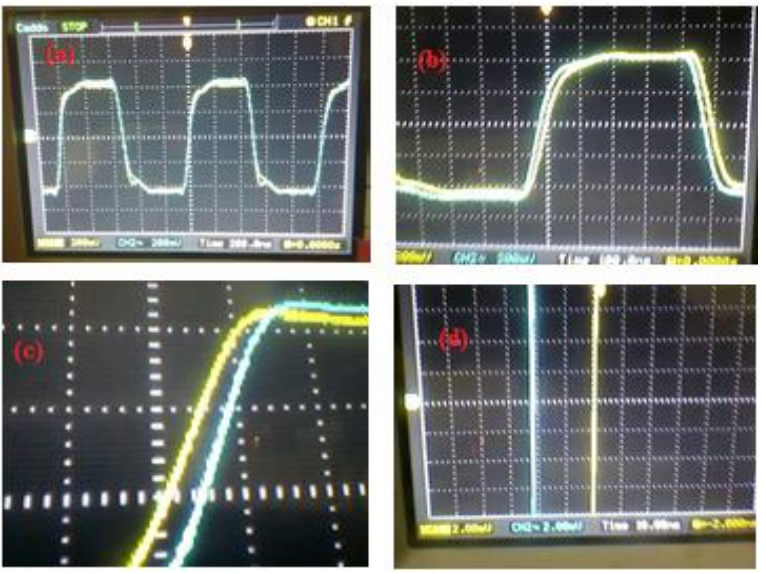

Figure 7. The phase shift between the signals: (a) The $\Pi=0$ and $\zeta=0$ at 200 ns/div time and 200 mV/div. (b) Phase difference in 200 mV/div and 100 ns/div, (c) Phase difference in 100 mV/div and 50 ns/div (d) Phase difference in 2 mV/div and 10 ns/div.

From the above scaling, the phase shift was fixed with an input sensitivity of 2 mV/div and 10 ns/div. This same sensitivity was adopted for measuring the phase shift of air, ethanol, distilled water and normal water using 20 mm electrodes. Figure 8(b) shows the delay time between air and ethanol, which is 7.8 ns. Figures 8(c) and 8(d) portray the delay time response for distilled water and normal water, respectively. The delay time for distilled water is 8 ns, while normal water has a delay time of 9 ns.

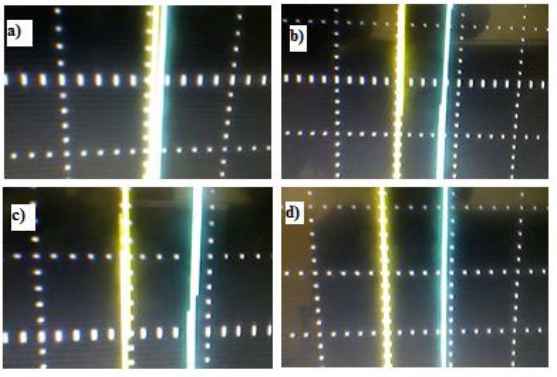

Figure 8. Phase shift between the signals from the 20 mm capacitance length: (a) Air (b) Ethanol (c) Distilled water (d) Normal water.

Next, the phase shift was measured using 40 mm electrodes for the same liquid samples. The results, shown in Figure 9, indicate that ethanol exhibits a delay time of 10 ns, distilled water 15 ns and normal water 18 ns. Additionally, when the phase shift of ethanol was measured using 70 mm electrodes, the delay time was 11 ns.

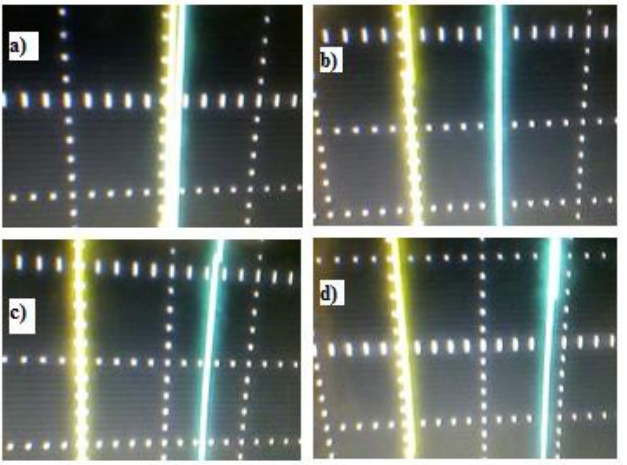

Figure 9. Phase shift between the signals from the 40 mm capacitance length (a) Air (b) Ethanol (c) Distilled water (d) Normal water.

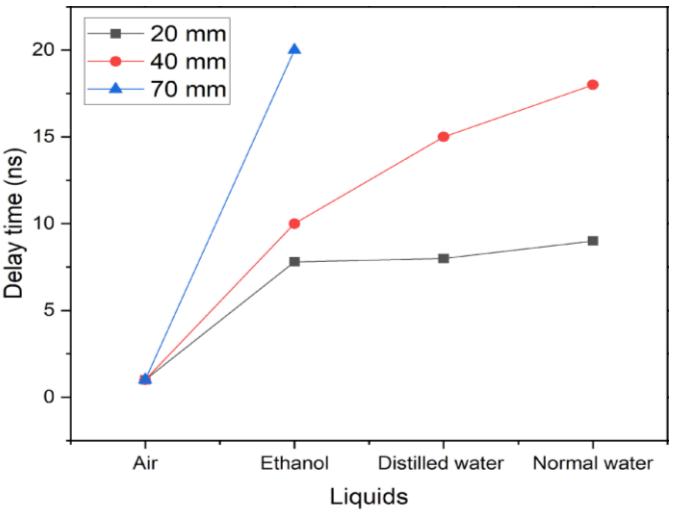

Figure 10. Comparison of the Delay time of the 20 mm, 40 mm and 70 mm Electrodes.

Comparison studies conducted for these three types of electrodes revealed that the capacitance sensor with 40 mm electrodes provides a more linear output for delay time compared to the 20 mm and 70 mm electrodes,

as evident from Figure 10. The phase shift and delay time calculated using Mathematica software for the 40 mm electrode-based capacitance sensor for three types of liquids are summarised in Table 2.

Table 2 Comparison of phase shift and response time of different types of liquids for 40 mm electrode.

Liquid	ε_e	Real Part of Admittance	Imaginary Part of Admittance	Phase $(\times 1000)$	Delay Time	Difference
Air (ref)	1	0.877316	1.18319	20.8233	57.8426	0
Ethanol	24	2.73782×10^{-6}	0.287157	5.05395	14.0388	43.8038
Distilled water	78	2.64233×10^{-8}	0.25928	4.56332	12.6759	45.1667
Normal Water	81	2.30777×10^{-8}	0.258856	4.55586	12.6552	45.1874

The calculated and measured values of phase shift and delay time for the 40 mm electrode-based capacitance sensor across three types of liquids are presented in Table 3. It can be observed that the 40 mm electrode-based capacitance sensor provides optimal measurable outputs for the three liquids with respect to air, closely aligning with the theoretical results. Thus, the 40 mm electrode capacitance sensor is a superior choice for measuring the void fraction in liquid/liquid phases. Similarly, the void fraction calculation was carried out for the gas/gas phases in the following sections.

Table 3: Experimental and calculated values for three liquids for a 40 mm electrode.

Liquid	ε_e		Phase shift in degrees		Response Time in ns		Difference in ns	
	Exp	Cal	Exp	Cal	Exp	Cal	Exp	Cal
Air (ref)	1	1	0	20.8233	0	57.8426	0	0
Ethanol	24	24	3.24	5.05395	9	14.0388	9	43.8038
Distilled Wafer	78	78	5.4	4.56332	15	12.6759	15	45.1667
Normal Wafer	81	81	6.48	4.55586	18	12.6552	18	45.1874

3.2 Phase-Shift Detection for Different Types of Gases

Phase detection was conducted for various gases using the same methodology applied to liquid/gas phases. The phase shift and response were calculated for five gases using 40 mm electrodes and Equation 5. The results are presented in Table 4.

Gas	ε_e	Real Part of admittance	Imaginary Part of admittance	Phase	Phase Difference	Response Time	Time Difference
AIR	1	0.877316	1.18319	20.8233	0	57.8426	0
N_2	1.47	0.190613	0.892688	15.711	5.1123	43.6416	14.201
CH_4	1.56	0.155105	0.86092	15.1519	5.6714	42.0887	15.7539
O_2	3.49	0.006737	0.527148	9.27774	11.5456	25.7715	32.0711
CO_2	12.6	0.00644275	0.325377	5.72663	15.0967	15.9073	41.9353
He	19.9	6.20991×10^{-6}	0.296371	5.21612	15.6072	14.4892	43.3534

Table 4: Calculated values of phase shift and response time of 40 mm electrode for five gases.

The phase shift was measured with an input sensitivity of 2 mV/div and 10 ns/div for two gases, Nitrogen (N_2) and Oxygen (O_2), using 20 mm, 40 mm and 110 mm electrodes. However, the delay time could not be measured with the 20 mm and 40 mm electrodes as it falls below the nanosecond range. Therefore, we selected an enhanced electrode length of 110 mm. The phase shift and response time were measured for Nitrogen and Oxygen using the same input sensitivity, with the experimental results illustrated in Figure 11. In this study, Nitrogen (N_2) exhibited a delay time of 2 ns and a phase shift of 0.72, while Oxygen (O_2) showed a delay time of 5 ns and a phase shift of 1.8.

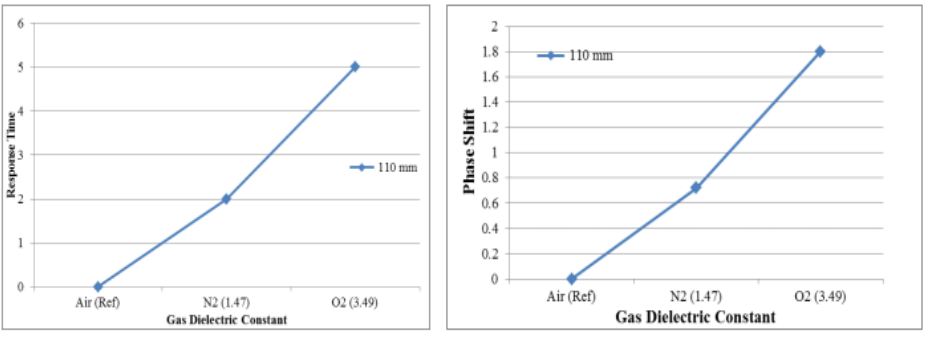

Figure 11: Phase Shift and Response Time of the Nitrogen and Oxygen gas for the 110 mm electrode capacitance sensor

To demonstrate the proposed concept on other gases, we tested ozone gas using three types of electrodes, yielding a response from the 110 mm electrodes, albeit with some noise due to the ozone gas generator. The experimental setup for detecting the phase shift of ozone gas is depicted in Figure 12. After introducing ozone into the glass tube, a time delay of 2.5 ns was measured, despite some noise. This study thus proves the versatility of the proposed method for void fraction detection of various types of gases.

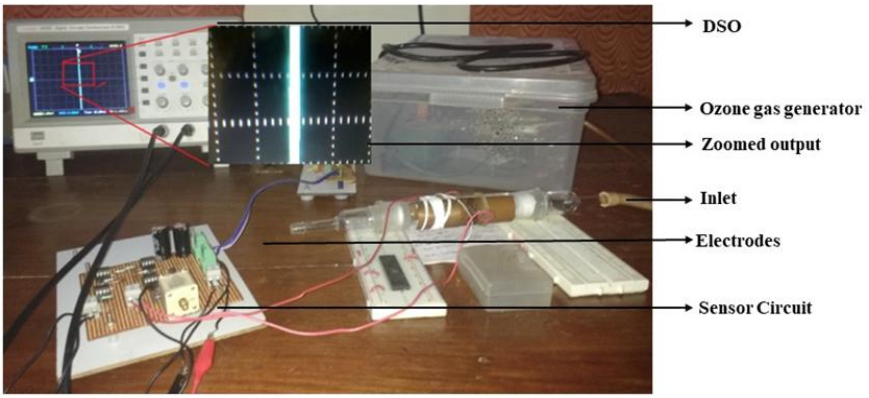

Figure 12: Setup of ozone gas with 110 mm electrodes.

4. Conclusion

A capacitance-based void fraction sensor was designed and developed to detect three different types of liquids and gases using electrodes of varying lengths: 20 mm, 40 mm and 70 mm. The phase shift and response time (delay time) were calculated and measured for three liquids. The calculated delay time for liquids was found to be linearly consistent with experimental results using 40 mm electrodes. The delay time was calculated for five gases using a porous medium of PSF with 80% MCM-41, employing 40 mm electrodes, resulting in very low delay times below the nanosecond range. Therefore, the delay time was measured using 110 mm electrodes for ozone, nitrogen and oxygen. The obtained delay times for nitrogen (N_2), oxygen (O_2) and ozone (O_3) were found as 2 ns, 5 ns and 3 ns, respectively. Consequently, the proposed method can be adopted for detecting void fractions of any liquid or gas with slight adjustments in the electrode length.

Acknowledgement

One of the authors, Kesavan Venkatachalam, gratefully acknowledges the University of Madras, Chennai, India, for awarding a scholarship under the Best Student category of the M.Phil. program.

Statements and Declarations

Funding

The authors declare that no funding, grants, or other financial support were received to carry out this work and the preparation of this manuscript.

Conflict of Interest

The corresponding author, on behalf of all co-authors, declares that there are no conflicts of interest.

Author's contributions

Kesavan Venkatachalam: Conceptualisation, Circuit design, Data Collections, Formal analysis, Investigation, Data Writing – original draft, Writing – review & editing.

J. Jayachandiran: Validation, Investigation, Formal analysis.

D. Nedumaran: Supervision, Scientific Analysis, Validation, Investigation.

References

[1] G. H. Roshani, E. Nazemi, S. A. H. Feghhi, and S. Setayeshi, "Flow regime identification and void fraction prediction in two-phase flows based on gamma ray attenuation," *Measurement (Lond)*, vol. 62, pp. 25–32, Jan. 2015, doi: 10.1016/j.measurement.2014.11.006.

[2] H. Canière *et al.*, "Horizontal two-phase flow characterization for small diameter tubes with a capacitance sensor," *Meas Sci Technol*, vol. 18, no. 9, pp. 2898–2906, Sep. 2007, doi: 10.1088/0957-0233/18/9/020.

[3] D. U. Lawal, "VOID FRACTION MEASUREMENT USING ELECTRICAL IMPEDANCE TECHNIQUES," 2014.

[4] M. Zubair and T. B. Tang, "A high resolution capacitive sensing system for the measurement of water content in crude oil," *Sensors (Switzerland)*, vol. 14, no. 7, pp. 11351–11361, Jun. 2014, doi: 10.3390/s140711351.

[5] A. Jaworek and A. Krupa, "Phase-shift detection for capacitance sensor measuring void fraction in two-phase flow," *Sens Actuators A Phys*, vol. 160, no. 1–2, pp. 78–86, 2010, doi: 10.1016/j.sna.2010.04.003.

[6] S Huang, J Fielden, R G Green, and M S Beck, "A new capacitance transducer for industrial applications," *J Phys E*, vol. 251, 3, no. 21, p. 2, 1988, doi: 10.1088/0022-3735/21/3/002.

[7] J. W. Schmidt and M. R. Moldover, "Dielectric Permittivity of Eight Gases Measured with Cross Capacitors," 2003.

[8] S. Kim, "High Permeability/High Diffusivity Mixed Matrix Membranes For Gas Separations," 2007.

[9] T. Wagner, S. Haffer, C. Weinberger, D. Klaus, and M. Tiemann, "Mesoporous materials as gas sensors," *Chem Soc Rev*, vol. 42, no. 9, pp. 4036–4053, Apr. 2013, doi: 10.1039/c2cs35379b.

[10] T. Wagner *et al.*, "A high temperature capacitive humidity sensor based on mesoporous silica," *Sensors*, vol. 11, no. 3, pp. 3135–3144, Mar. 2011, doi: 10.3390/s110303135.

[11] A. Prim, E. Pellicer, E. Rossinyol, F. Peiró, A. Cornet, and J. R. Morante, "A novel mesoporous CaO-loaded in2O3 material for CO2 sensing," *Adv Funct Mater*, vol. 17, no. 15, pp. 2957–2963, Oct. 2007, doi: 10.1002/adfm.200601072.

[12] B. Yuliarto, I. Honma, Y. Katsumura, and H. Zhou, "Preparation of room temperature NO 2 gas sensors based on W- and V-modified mesoporous MCM-41 thin films employing surface photovoltage technique," *Sens Actuators B Chem*, vol. 114, no. 1, pp. 109–119, Mar. 2006, doi: 10.1016/j.snb.2005.04.016.

[13] J. Yang *et al.*, "An enhanced gas sensor based on SiO2@mesoporous MCM-41 core-shell nanocomposites for SO2visual detection," *Analyst*, vol. 145, no. 12, pp. 4352–4357, Jun. 2020, doi: 10.1039/d0an00621a.

[14] S. Esmaeili, M. A. Zanjanchi, H. Golmojdeh, and S. Shariati, "Modification of MCM-410-Based Core-Shell for Construction of a Colorimetric Gas Sensor," *IEEE Sens J*, vol. 21, no. 16, pp. 17665–17672, Aug. 2021, doi: 10.1109/JSEN.2021.3052880.

[15] R. Qi *et al.*, "Humidity sensors based on MCM-41/polypyrrole hybrid film via in-situ polymerization," *Sens Actuators B Chem*, vol. 277, pp. 584–590, Dec. 2018, doi: 10.1016/j.snb.2018.09.062.